Neutral-Pion Electroproduction on the Proton near Threshold

H. B. van den Brink,[1] H. P. Blok,[1] I. Bobeldijk,[2] M. Bouwhuis,[2] G. E. Dodge,[1] M. N. Harakeh,[1,*] W. H. A. Hesselink,[1] D. G. Ireland,[2,†] C. W. de Jager,[2] E. Jans,[2] N. de Jonge,[2] N. Kalantar-Nayestanaki,[1,*] W-J. Kasdorp,[2] T. J. Ketel,[1] J. Konijn,[2] L. Lapikás,[2] J. J. van Leeuwe,[2] R. L. J. van der Meer,[2] G. J. L. Nooren,[2] B. E. Norum,[3] E. Passchier,[2] A. R. Pellegrino,[1] C. M. Spaltro,[1] G. van der Steenhoven,[2] J. J. M. Steijger,[2] J. A. Templon,[1] J. A. P. Theunissen,[2] M. A. van Uden,[2] H. de Vries,[2] R. de Vries,[2] and P. K. A. de Witt Huberts[2]

[1]*Department of Physics and Astronomy, Vrije Universiteit, De Boelelaan 1081, NL-1081 HV Amsterdam, The Netherlands*

[2]*Nationaal Instituut voor Kernfysica en Hoge-Energiefysica (NIKHEF, sectie K), P.O. Box 41882, NL-1009 DB Amsterdam, The Netherlands*

[3]*University of Virginia, Charlottesville, Virginia 22901*

(Received 6 January 1995)

The double-differential coincidence cross section for the reaction $^1\mathrm{H}(e,e'p)\pi^0$ has been measured at $Q^2 = 0.1$ (GeV/c)^2 in a range in the invariant mass of 2–14 MeV above threshold. From the angular dependence of the data values of the pion s-wave multipoles E_{0+} and L_{0+} have been extracted. The results are compared to predictions from chiral perturbation theory and models based on an effective Lagrangian. None of the models is able to describe both the E_{0+} and the L_{0+} multipoles.

PACS numbers: 25.30.Rw, 11.40.Ha, 12.39.Fe, 13.60.Le

The production of a π^0 meson on the proton near threshold is of fundamental interest as a test of our knowledge of the strong interaction at low energies. At threshold the reaction is determined by the s-wave multipoles E_{0+} and L_{0+}. Several theories predict the values of these multipoles. The low energy theorem (LET) [1–6], which is based on gauge invariance, partial conservation of axial current (PCAC), crossing symmetry, and analyticity, makes a prediction for the values of E_{0+} and L_{0+} at threshold up to order μ^2, with $\mu = m_\pi/m_p$, where m_π and m_p are the masses of the pion and the proton, respectively. For electroproduction, the range of validity of the LET is limited to rather small values of $Q^2 = -q^2$, where q is the transferred four momentum. Chiral perturbation theory (ChPT) [7] uses an effective πN Lagrangian, which includes the above mentioned symmetries, in which the effect of chiral-symmetry breaking is treated in a perturbative fashion. It can calculate observables to higher orders in μ, and thus includes the LET. On account of its structure ChPT can make predictions at values of the invariant mass W of the πN system also away from threshold, and at nonzero values of Q^2. Finally, there are pion-nucleon models, using an effective πN Lagrangian [8–10]. In these models pion-production operators [11,12], which are based on Born plus delta-isobar (Δ) terms, are used. The models include πN rescattering via a πN potential or Watson's theorem [13].

Photoproduction (γ,π^0) experiments [14,15] have generated a lot of excitement, because the first analysis of the data suggested that the value of the E_{0+} multipole was significantly different from the LET prediction. An important item in the discussion was how to account for the effect of the $(\gamma,\pi^+)(\pi^+,\pi^0)$ charge-exchange channel and, related to this, the threshold at which the LET should be applied (the π^+ threshold lies 5.9 MeV above the one for π^0 production). The consensus now is that LETs have to be applied at their own physical threshold. Furthermore, all analyses, though indicating that the value of E_{0+} varies considerably with the invariant mass W, are consistent with the LET prediction at the π^0 threshold [16–18]. In this context it should be remarked that there is discussion about the validity and practical use of these "old" LETs [19].

The first electroproduction experiment near threshold was performed at NIKHEF [20]. The total cross section for the $^1\mathrm{H}(e,e'p)\pi^0$ reaction was measured at $Q^2 = 0.05$ and 0.10 (GeV/c)^2. It yielded the value of $a_0 = |E_{0+}|^2 + \epsilon_L|L_{0+}|^2$ close to threshold, where $\epsilon_L = \epsilon Q^2/\omega^{*2}$, with ϵ the virtual-photon polarization, and ω^* the energy of the virtual photon in the π-p center of mass (c.m.) frame. With reasonable assumptions extrapolation to $Q^2 = 0$ yielded a value of L_{0+} in agreement with the LET prediction [20]. Calculations in ChPT also gave a good description of the measured Q^2 dependence of a_0 [21].

The purpose of the present work is to study the behavior of the E_{0+} and L_{0+} multipoles separately, and as a function of W. This is done by measuring the pion angular distribution in the $^1\mathrm{H}(e,e'p)\pi^0$ reaction for values of W from threshold to about 14 MeV above it. In this way it becomes possible to confront the various models for the prediction of π^0 production at low energies with detailed data, especially around the important π^+ threshold.

The coincidence cross section for the $(e,e'\pi^0)$ reaction can be written as $d^3\sigma/dE_{e'}\,d\Omega_{e'}\,d\Omega^*_\pi = \Gamma_v\, d\sigma/d\Omega^*_\pi$ [18], with Γ_v the virtual photon flux. The pion production cross section in the c.m. frame $d\sigma/d\Omega^*_\pi$ can be expressed

in terms of four structure functions R, which depend on W, Q^2, and θ_π^*, the c.m. polar angle of the pion with respect to the transferred three momentum $\vec{q}$,

$$\frac{d\sigma}{d\Omega_\pi^*} = \frac{p_\pi^*}{q_L}\frac{W}{m_p}[R_T + \epsilon_L R_L + \epsilon\cos(2\phi_\pi^*)R_{TT} + \sqrt{2\epsilon_L(\epsilon+1)}\cos\phi_\pi^* R_{LT}], \quad (1)$$

with ϕ_π^* the c.m. azimuthal angle of the pion with respect to $\vec{q}$, p_π^* the c.m. momentum of the pion, and $q_L = (W^2 - m_p^2)/2m_p$.

Assuming only s and p waves for the pion this expression reduces to

$$\frac{d\sigma}{d\Omega_\pi^*} = \frac{p_\pi^*}{q_L}\frac{W}{m_p}\{A + B\cos\theta_\pi^* + C\sin\theta_\pi^*\cos\phi_\pi^* + D\cos^2\theta_\pi^* + E\sin^2\theta_\pi^*\cos(2\phi_\pi^*)\}. \quad (2)$$

The coefficients A, B, and C can be written in terms of the s- and p-wave multipoles,

$$\begin{aligned} A &= \epsilon_L|L_{0+}|^2 + |E_{0+}|^2 + \tfrac{1}{2}|3E_{1+} - M_{1+} + M_{1-}|^2 + \tfrac{1}{2}|2M_{1+} + M_{1-}|^2, \\ B &= 2\,\mathrm{Re}\{E_{0+}^*(3E_{1+} + M_{1+} - M_{1-})\}, \\ C &= -\sqrt{\epsilon_L(\epsilon+1)}\,\mathrm{Re}\{L_{0+}^*(3E_{1+} - M_{1+} + M_{1-})\}. \end{aligned} \quad (3)$$

In these expressions we neglected the contribution from the L_{1-} and L_{1+} multipoles, which are relatively small in the discussed models in our kinematical regime. The coefficients D and E are combinations of p-wave multipoles only.

By measuring the cross section at $\theta_\pi^* = 0°$ and 180° and at $(\theta_\pi^*, \phi_\pi^*) = (90°, 0°)$ and $(90°, 180°)$ the values of B and C can be determined. Since the imaginary parts of the p-wave multipoles are small near threshold, the real part of the values of the E_{0+} and the L_{0+} multipoles can be extracted if one has a reliable estimate of the relevant combinations of p-wave multipoles.

The experiment was performed at NIKHEF-K with the extracted electron beam from the Amsterdam Pulse-Stretcher (AmPS) ring [22] and the two-spectrometer setup [23]. Data were taken at an incident electron energy of 525 MeV with a current of 10 μA and a duty factor of 30%. The angle of the scattered electron was 45.4°, giving $Q^2 = 0.10$ (GeV/c)^2 and $\epsilon = 0.67$.

The scattered electron was detected in the quadrupole-dipole-dipole (QDD) spectrometer. The detection of a π^0 particle was avoided by detecting the recoiling proton in the quadrupole-dipole-quadrupole (QDQ) spectrometer instead. Close to threshold the proton has a low kinetic energy in the c.m. frame. Therefore, in the laboratory frame the proton will be emitted in a cone centered on $\vec{q}$, with an opening angle that depends on W. Since the QDQ spectrometer in which the proton is detected has a relatively large solid angle, it is possible to measure in one setting a considerable fraction of the π^0 angular distribution. Measurements were performed at central values $\theta_\pi^* = 0°$ and 180°, and at $(\theta_\pi^*, \phi_\pi^*) = (90°, 0°)$ and $(90°, 180°)$.

A cryogenic H_2 target [24] with a length of 10 cm was used, operated just above the critical point at 35 K and 15 bars. The resulting density of 22 mg/cm^3 was a compromise between count rate and loss of resolution due to the straggling of the protons in the target. The acceptance along the beam line of the coincidence setup was limited by the electron spectrometer to 2.5 cm, which determined the effective target thickness to be about 55 mg/cm^2. The product of accumulated charge (Q) and target thickness (t) was calibrated by measuring elastic ^{1}H(e,e) scattering with the electron spectrometer, positioned at the same angle as during the π^0 measurement. Concurrently, the number of single protons in the QDQ spectrometer was measured at the same settings as during the π^0 measurements. In this way the number of proton singles acted as a monitor on the luminosity $Q \times t$ during the π^0 runs.

The coincidence efficiency of the detector setup was determined to be 0.99 ± 0.01 by measuring elastic ^{1}H$(e,e'p)$ scattering with a CH_2 target. Detection efficiencies of the spectrometers were 0.94 for the QDQ and 0.97 for the QDD. The dead time in the QDQ was 1.7%, while in the QDD it was smaller than 0.1%. The final systematic error on the cross section is 4%.

The analysis of the data included the following steps: (1) reconstruction of the momentum vectors of the particles in the vertex by using the optical properties of the spectrometers; (2) calculation of W and Q^2 from the reconstructed electron momentum vector. The FWHM resolution was 2×10^{-3} (GeV/c)^2 in Q^2 and 0.8 MeV in W; (3) calculation of θ_π^* and ϕ_π^* from W, Q^2, and the reconstructed proton and electron momentum vectors. Depending on the kinematics the resolution varied, for θ_π^* from 6° to 10° and for ϕ_π^* from 11° to 24°; (4) correction of the time of detection of the particles for path length differences, which resulted in a coincidence time (t_c) resolution of 1 ns; (5) calculation of the missing mass E_m from the particle momenta and energies, which yielded a peak at 135 MeV, with a width of 1.4 to 3.5 MeV, depending on the kinematics; (6) binning of the data in W, θ_π^*, and ϕ_π^* with windows on t_c and E_m; (7) subtraction of accidental coincidences using a proper window on t_c; (8) division by $Q \times t$, efficiency factors, dead time corrections, and by the detection volume to obtain the differential cross section. The acceptance of the detector setup (detection volume) was calculated with a Monte Carlo method by using the program GEANT [25]. Finally, the cross section was corrected for radiation losses [26].

The extracted cross sections as a function of θ_π^* for $\phi_\pi^* = 0°$ and $\phi_\pi^* = 180°$ are presented in Fig. 1 in two W ranges. The large difference between $\phi_\pi^* = 0°$ and 180° indicates a large value of the R_{LT} structure function. A fit was made to the data for each W bin of 1 MeV width, using Eq. (2). The fit of the coefficients D and E resulted in values per W bin that were small with large errors. Therefore, since D and E are combinations of p-wave multipoles, their energy dependence was parametrized as

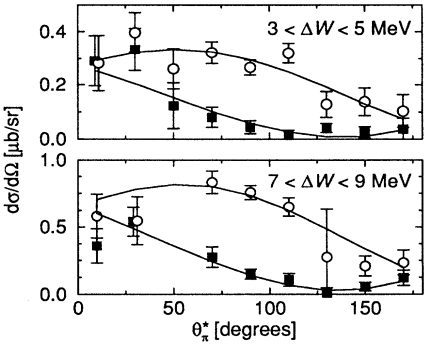

FIG. 1. Measured cross sections as a function of θ_π^* in the range $-30° < \phi_\pi^* < 30°$ (solid squares) and $150° < \phi_\pi^* < 210°$ (empty circles) in two ΔW bins, where ΔW is the value of W above threshold. The lower and upper curves represent the fit to the data for $\phi_\pi^* = 0°$ and 180°, respectively.

$D = dp_\pi^{*2}$ and $E = ep_\pi^{*2}$. The values thus obtained, $d = (-0.73 \pm 0.51) \times 10^{-4}$ μb/(sr MeV^2) and $e = (-0.12 \pm 0.46) \times 10^{-4}$ μb/(sr MeV^2), were used to constrain D and E in the final fit. The small values of d and e are consistent with the fact that in most model calculations $M_{1+}/M_{1-} \approx -2$, which yields $d, e \approx 0$. The solid curves in Fig. 1 represent the results of the fit to the data for $\phi_\pi^* = 0°$ (lower curve) and $\phi_\pi^* = 180°$ (upper curve). The fitted coefficients A, B, and C are plotted in Fig. 2.

The coefficient A can be parametrized as $a_0 + bp_\pi^{*2}$, where a_0 represents the s-wave part and the second term the contribution from p waves. The values of a_0 and b determined in this way were $a_0 = 0.390 \pm 0.042$ μb/sr and $b = (0.444 \pm 0.028) \times 10^{-3}$ μb/(sr MeV^2). These values are in good agreement with the values $a_0 = 0.353 \pm 0.087$ and $b = 0.4 \pm 0.1$, determined by Welch *et al.* [20] and Brauel *et al.* [27], respectively. The parametrization is indicated with the solid curve in the top panel of Fig. 2.

The curves in Fig. 2 represent the results of several theoretical predictions. The dotted curves are the result of a calculation by Blaazer [10,28], who uses the Dressler operator [12]. In this case no rescattering was included. The dashed curves are due to Lee [29]. Both calculations include the Born terms with some minor effects due to vector-meson exchange and contributions from the Δ resonance. Watson's theorem [13] was used to account for rescattering in the calculations by Lee. The dash-dotted curves represent results from a calculation by Davidson [9,30], in which the same terms as above are evaluated. A K-matrix approach [17], consistent with Watson's theorem, was used to estimate the energy dependence of the E_{0+} multipole. Apart from this, this calculation's main difference with the others is that it is relativistic and that the crossed Δ term is also taken into account in the calculation. The open diamonds represent the relativistic ChPT predictions [7,31]. In these calculations all the tree and one-loop diagrams have been evaluated, and the different thresholds for π^0 and π^+

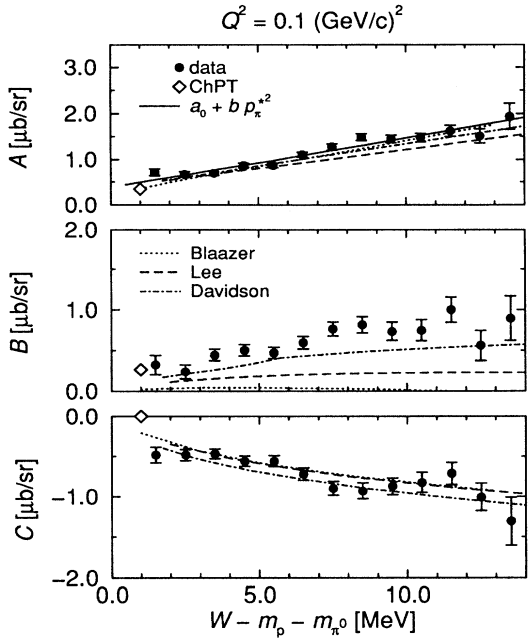

FIG. 2. Coefficients A, B, and C, obtained from fitting Eq. (2) to the measured cross sections, with the terms D and E constrained as described in the text, compared to the results of theoretical calculations.

have been taken into account. It should be noted that the one-loop corrections become rather large at this Q^2 [7].

All calculations give a fair description of the A term. However, none of the calculations describes both the value of C (representing the interference structure function R_{LT}, which is proportional to L_{0+}) and the value of B (representing the $\cos\theta_\pi^*$ term in the cross section, proportional to E_{0+}). The calculation by Davidson gives the best description of all the terms.

For the extraction of E_{0+} and L_{0+} from the experimentally determined values of B and C [see Eq. (3)] we used a recent LET prediction [32] for the value of the p-wave multipoles. Since the values for the relevant p-wave combinations calculated by Blaazer and Davidson within their models differ by less than about 10% from these values, the model dependence in the resulting values of E_{0+} and L_{0+} is estimated to be about 10%. The values of the thus extracted real parts of E_{0+} and L_{0+} are presented in Fig. 3. With respect to the value at the photon point, E_{0+} has changed sign and its value is now positive.

It is interesting to investigate whether our data give indication for a variation of the multipoles with W as was observed for E_{0+} in the photoproduction case. The solid curve in Fig. 3 represents the value of E_{0+} at $Q^2 = 0$ taken from Ref. [16], shifted upwards by $2.7 \times 10^{-3}/m_{\pi^+}$ to globally account for the change in Q^2, according to Ref. [6]. If at all, our data point to a smaller variation with W. However, our values for L_{0+} clearly show a variation around the π^+ threshold. This variation in L_{0+} (as observed in the C term) is not described by any model.

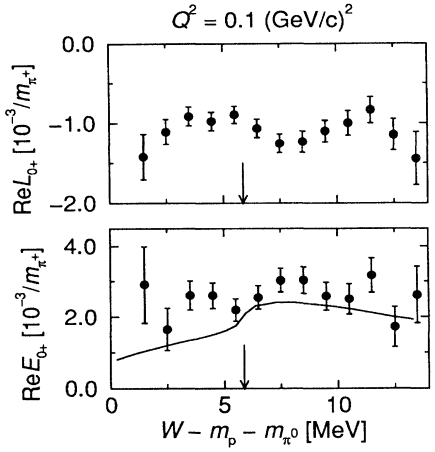

FIG. 3. Values of $\mathrm{Re}E_{0+}$ and $\mathrm{Re}L_{0+}$ at $Q^2 = 0.1$ (GeV/c)^2 as a function of W. The solid curve represents values of E_{0+} at the photon point, shifted upwards by 2.7 units. The arrows indicate the position of the $(\pi^+ n)$ threshold.

In summary, differential cross sections near threshold for the reaction $^1\mathrm{H}(e,e'p)\pi^0$ have been measured, made possible by the high duty factor of the beam, extracted from the AmPS ring, in combination with the high momentum and angular resolution of the detectors. The cross section was determined in a range in invariant mass W of 2–14 MeV above the π^0 threshold. No theoretical calculation is able to describe simultaneously the $\cos\phi^*_\pi$ dependent term in the cross section, which depends on the L_{0+} multipole, and the $\cos\theta^*_\pi$ term, which depends on the E_{0+} multipole.

From the data the real parts of the values of the E_{0+} and L_{0+} multipoles have been extracted, using a recent LET p-wave prediction to estimate the contribution of the p-wave multipoles. The data indicate a variation of L_{0+} with W around the π^+ threshold. This variation is not described by any model, presumably due to the fact that the charge-exchange contribution is not taken into account explicitly.

The work described in this paper is part of the research program of the "Stichting voor Fundamenteel Onderzoek der Materie (FOM)," which is financially supported by the "Nederlandse Organisatie voor Wetenschappelijk Onderzoek (NWO)." The authors would like to thank V. Bernard, F. Blaazer, R. Davidson, T.-S. H. Lee, and U.-G. Meißner for useful discussions and for providing us with the results of their calculations. We would like to thank J. F. J. van den Brand and O. Unal for the use of the target.

*Present address: KVI, Zernikelaan 25, 9747 AA Groningen, The Netherlands.
†Present address: Department of Physics and Astronomy, University of Glasgow, Glasgow G12 8QQ, United Kingdom.

[1] N. M. Kroll and M. A. Ruderman, Phys. Rev. **93**, 233 (1954).
[2] Y. Nambu and E. Shrauner, Phys. Rev. **128**, 862 (1962).
[3] S. Fubini and G. Furlan, Ann. Phys. **48**, 322 (1968).
[4] P. de Baenst, Nucl. Phys. **B24**, 633 (1970).
[5] A. I. Vainshtein and V. I. Zakharov, Nucl. Phys. **B36**, 589 (1972).
[6] S. Scherer and J. H. Koch, Nucl. Phys. **A534**, 461 (1991).
[7] V. Bernard, N. Kaiser, T.-S. H. Lee, and U.-G. Meißner, Phys. Rep. **246**, 315 (1994).
[8] S. Nozawa, B. Blankleider, and T.-S. H. Lee, Nucl. Phys. **A513**, 459 (1990).
[9] R. M. Davidson, Czech. J. Phys. **44**, 365 (1994).
[10] F. Blaazer, B. L. G. Bakker, and H. J. Boersma, Nucl. Phys. **A568**, 681 (1994); F. Blaazer, Ph.D. thesis, Vrije Universiteit, Amsterdam, 1995.
[11] I. Blomqvist and J. M. Laget, Nucl. Phys. **A280**, 405 (1977).
[12] E. T. Dressler, Can. J. Phys. **66**, 279 (1988).
[13] K. M. Watson, Phys. Rev. **95**, 228 (1954).
[14] E. Mazzucato *et al.,* Phys. Rev. Lett. **57**, 3144 (1986).
[15] R. Beck *et al.,* Phys. Rev. Lett. **65**, 1841 (1990).
[16] J. Bergstrom, Phys. Rev. C **44**, 1768 (1991).
[17] A. M. Bernstein and B. R. Holstein, Comments Nucl. Part. Phys. **20**, 197 (1991).
[18] D. Drechsel and L. Tiator, J. Phys. G **18**, 449 (1992).
[19] G. Ecker and U.-G. Meißner, Comments Nucl. Part. Phys. (to be published).
[20] T. P. Welch *et al.,* Phys. Rev. Lett. **69**, 2761 (1992).
[21] V. Bernard, N. Kaiser, T.-S. H. Lee, and U.-G. Meißner, Phys. Rev. Lett. **70**, 387 (1993).
[22] P. K. A. de Witt Huberts, Nucl. Phys. **A553**, 845c (1993).
[23] C. de Vries *et al.,* Nucl. Instrum. Methods Phys. Res., Sect. A **223**, 1 (1984).
[24] O. Unal and J. F. J. van den Brand, University of Wisconsin, Internal Report, 1992.
[25] GEANT team, *GEANT-Detector Description and Simulation Tool* (CERN, Geneva, Switzerland, 1993) June 1993 ed., version 3.15.
[26] E. N. M. Quint, Ph.D. thesis, Universiteit van Amsterdam, 1988.
[27] P. Brauel *et al.,* Phys. Lett. **50B**, 507 (1974).
[28] F. Blaazer (private communication).
[29] T.-S. H. Lee (private communication).
[30] R. M. Davidson (private communication).
[31] V. Bernard and U.-G. Meißner (private communication).
[32] V. Bernard, N. Kaiser, and U.-G. Meißner, Phys. Rev. Lett. (to be published).